WISM484 - Utrecht University Third Assignment

Spontaneous Synchronization in the Kuramoto Model

Introduction to Complex Systems

Contents

The *synchronization* phenomenon for an oscillators population can be recognized in many different contexts and can be modelled with a great degree of confidence by a non-linear interaction between the oscillators. The goal of the this project is to investigate Kuramoto model for spontaneous synchronization in a oscillators system by means of both theoretical and experimental tools.

The present work is subdivided in three main blocks: a theoretical investigation of the Kuramoto model in the first part (Sec.2) that will provide the foundation for critical analysis of the model, suggesting some analogy with the XY ferromagnetic model for an interacting spins system (Sec.2.4); a simulation of the Kuramoto model for different starting configurations (Sec.3) which is meant to validate the theoretical analysis in Sec.2; a simulation and discussion on the Kuramoto model on a Watts-Strogatz graphs (Sec.4).

All bibliographic references perused for this report is available on `GitHub` together with all

Sergio Picella
6641334

the code produced and run.

1 Introduction

In a population of mutually interacting oscillators, the time-evolution dynamics for given coupling forces parameters and initial distribution can lead the whole system to synchronize and converge to an equilibrium state: depending on the starting conditions and coupling forces, a common phase and average frequency can be shared between most of of the oscillators, regardless on the natural frequency of the individual oscillator.
The Kuramoto model[1] (1975) can efficiently describe synchronizations and critical behaviour of such systems (e.g. [2],[3]). This model is based on the following main hypothesis: given a set of N oscillators with phase $\boldsymbol{\theta}(t) = [(\theta_1(t), \ldots, \theta_N(t)]$ and natural frequencies $\boldsymbol{\omega}(t) = [\omega_1(t), \ldots, \omega_N(t)]$ and a NxN matrix of mutual interactions coupling strengths $\boldsymbol{K}$, the evolution of the systems can be evaluated by mean of the following set of differential equations:

$$\frac{d\theta_i(t)}{dt} = \omega_i(t) + \sum_j^N K_{i,j} \sin\big(\theta_j(t) - \theta i(t)\big), \qquad \forall i, j = 1, \ldots, N \tag{1}$$

where $K_{i,j} = 0$ if the i-th and j-th oscillators are not interacting.
For this assignment the following assumption has been made on the model in Eq.1:

$$K_{i,j} = \frac{K}{N}, \qquad K \text{ const}\,; \forall i, j \in 1, \ldots, N \tag{2}$$

This assumption results in a uniform distribution of coupling interaction weights between the oscillators and it is often referred to as *mean-field Kuramoto* approximation, with K being the coupling constant. Moreover, made exception for Sec.4, the lattice of interacting oscillators will be assumed to be fully connected, namely each oscillator will be interacting with every other one. The dynamic of the system resulting from these hypotheses is therefore described by:

$$\frac{d\boldsymbol{\theta}(t)}{dt} = \boldsymbol{\omega} + \frac{K}{N} \sum_j^N \sin\big(\theta_j(t) - \theta i(t)\big), \qquad \forall i, j = 1, \ldots, N \tag{3}$$

2 Theoretical Exercises

The existence of $\overline{\omega}$ *mean natural frequency* will be justified and exploited to derive a compact expression for the Hamiltonian $\mathcal{H}$ of the Kuramoto oscillators systems with the addition of a *frustration* term. An analysis over the stability of this configuration will follow and stationary solutions will be defined. This whole process will lead to an apparent analogy with the *mean-field* Heisenberg XY ferromagnetic model which will be discussed.

2.1 Common frequency of the phase locked component

STATEMENT #1:

Given $\overline{\omega} = \frac{1}{N}\sum_{i=1}^{N}\omega_i$, prove that:

$$\frac{d}{dt}\left(\frac{1}{N}\sum_{i=1}^{N}\theta_i(t)\right) = \overline{\omega} \tag{4}$$

Proof. Note that:

$$\frac{d}{dt}\left(\frac{1}{N}\sum_{i=1}^{N}\theta_i(t)\right) = \frac{1}{N}\sum_{i=1}^{N}\dot{\theta}_i(t) \overset{Eq.3}{=} \frac{1}{N}\sum_{i=0}^{N}\left[\omega_i + \cancel{\frac{K}{N}\sum_{j=1}^{N}\sin(\theta_j(t)-\theta_i(t))}\right] = \frac{1}{N}\sum_{i}^{N}\omega_i = \overline{\omega}$$

where the mutual interaction term cancels out because the *sine* function is odd and the sum includes terms in the form $\sin(\theta_j(t) - \theta_i(t) + \sin(\theta_i(t) - \theta_j(t)\,\forall\, i,j = 1,\ldots,N$. □

Comment: The closer the system to a global synchronization of the oscillators, the smaller to the standard deviation of the $\frac{d\boldsymbol{\theta}}{dt}$ will be as more and more oscillators will rotate at the same common shared frequency $\overline{\omega}$.

2.2 Lyapunov function and *frustrated* Kuramoto model

By considering a rotating frame with frequency $\overline{\omega}$, the variable $\boldsymbol{\phi}(t) = [\phi_1(t),\ldots,\phi_N(t)]$ where $\phi_i(t) = \theta_i(t) - \overline{\omega}t\ \forall\, i = 1,\ldots,N$: can be introduced. This new variable can be used in a different expression for Kuramoto model, namely:

$$\frac{d\phi_i(t)}{dt} = (\omega_i - \overline{\omega}) + \frac{K}{N}\sum_{j=1}^{N}\sin(\phi_j(t) - \phi_i(t)), \qquad \forall\, i = 1,\ldots,N. \tag{5}$$

As an additional hyphotesis for the basic Kuramoto model in Eq.3, it is meaningful at this

point to introduce the

$$\mathcal{H}(\boldsymbol{\phi}(t), \boldsymbol{\omega}) = -\frac{K}{2N} \sum_{i=1,j=1}^{N} \cos(\phi_i(t) - \phi_j(t)) \; - \sum_{i=1}^{N} (\omega_i - \overline{\omega})\phi_i(t) \tag{6}$$

Hamiltonian function which describes the global energy of the system of Kuramoto oscillators. In Eq.Eq.6, it is possible on the one hand to recognize the first term to be responsible for decreasing in the total energy of the system if all the phases are the same (just like in the basic Kuramoto model); on the other hand, the second term takes into account a so called *frustration*, namely an increase of energy due to a random field depending on the $\boldsymbol{\omega}$ distribution and $\boldsymbol{\phi}(t)$ which tries to push the system far from a phase locked condition.

Extreme points of the Lyapunov function

STATEMENT #2:

Prove that $\mathcal{H}$ is a Lyapunov function, namely

$$\frac{d\mathcal{H}}{dt} = \sum_{i=1}^{N} \frac{\partial \mathcal{H}}{\partial\big(\phi_i(t)\big)} \frac{d\big(\phi_i(t)\big)}{dt} \leq 0 \tag{7}$$

for any $\boldsymbol{\phi}$.

Proof. Noting that

$$-\frac{\partial \mathcal{H}}{\partial\big(\phi_i(t)\big)} = (\omega_i - \overline{\omega}) - \frac{K}{N} \sum_{j=1}^{N} \sin\big(\phi_i(t) - \phi_j(t)\big) = \dot{\phi}_i(t) \implies -\nabla\mathcal{H} = \dot{\boldsymbol{\phi}}(t)$$

When studying then the $\frac{d\mathcal{H}}{dt}$, it follows by combining Eq.7 with Eq.2.2 that:

$$\begin{aligned} \frac{d\mathcal{H}}{dt} &= \sum_{i=1} \frac{\partial \mathcal{H}}{\partial\big(\phi_i(t)\big)} \frac{d\big(\phi_i(t)\big)}{dt} \\ &= \sum_{i=1} \frac{\partial \mathcal{H}}{\partial\big(\phi_i(t)\big)} \cdot \left(- \frac{\partial \mathcal{H}}{\partial\big(\phi_i(t)\big)} \right) \\ &= -\sum_{i=1}^{N} \left(\frac{\partial \mathcal{H}}{\partial\big(\phi_i(t)\big)} \right)^2 = -\Big(\nabla \mathcal{H} \Big)^2 \end{aligned} \tag{8}$$

□

Comment: This proof shows that the given dynamics for the Kuramoto model with frustration results in a decreasing energy over time, namely the system tends to a global minimization of the energy (if this minimum/a exist(s): this point will be discussed in next proof).

2.3 Stationary solutions of the Kuramoto model

STATEMENT #3:

Find the equations for the *extreme points* of $\mathcal{H}$.
Is the configuration with $\omega_i = \overline{\omega}\,\forall i = 1, \dots, N$ an asymptotically stable equilibrium?

Proof. An extreme point can be found by solving

$$0 = \nabla\mathcal{H} \iff 0 = (\omega_i - \overline{\omega}) - \frac{K}{N}\sum_{j=1}^{N}\sin\big(\phi_i(t) - \phi_j(t)\big), \forall i = 1, \dots, N$$

The extreme points for $\mathcal{H}$ are therefore given by:

$$\omega_i = \overline{\omega} + \frac{K}{N}\sum_{j=1}^{N}\sin(\phi_i(t) - \phi_j(t))]$$

Note at this point that if $\omega_i = \overline{\omega}$, the equilibrium conditions yields:

$$\frac{K}{N}\sum_{j=1}^{N}\sin(\phi_i(t) - \phi_j(t)) = 0$$

and if the sum over $i = 1, \dots, N$ is considered, the extreme point for $\mathcal{H}$ imposes that

$$0 = \nabla\mathcal{H} = \sum_{i=1}^{N}\left[\cancel{\frac{K}{N}\sum_{j=1}^{N}\sin(\phi_i(t) - \phi_j(t))}\right] \tag{9}$$

where again the sum over the interaction term cancels out being sine an odd function. Even though an equation for the fixed points has been found, this last result does not guarantee that, if the condition $\omega_i = \overline{\omega}$ is met, an asymptotically stable fixed point has been found. In the fixed points in fact $\nabla\mathcal{H} = 0$, but for the characterization of the fixed point (being it asymptotically stable equilibrium or unstable equilibrium) a different kind of analysis is needed and will follow in Sec.2.4. □

Comment: From the analytical point of view, as $\mathcal{H}$ is a Lyapunov function, fixed points correspondent to the minimum energy configurations (compare with following proofs) are asymptotically stable. As a side note, as it was suggested in [7], it is possible to numerically

observe metastability in the simulations, mostly caused by finite-size effects, if loops of increasing and decreasing `K` are simulated.

Stationary solutions and order parameter

STATEMENT #4:

If we introduce the order parameter:

$$r(t)\, e^{\mathrm{i}\Psi(t)} = \frac{1}{N}\sum_{j=1}^{N} e^{\mathrm{i}\phi_j(t)} \tag{10}$$

show that the stationary solutions of the Kuramoto model satisfies:

$$\Delta(\omega_i) = \omega_i - \overline{\omega} = K\, r\, sin\big(\phi_i - \Psi\big)$$

at the steady state.

Proof. Considering the steady state $\forall\, i = 1, \ldots, N$:

$$\begin{aligned}
\dot{\phi}_i &= \omega_i - \overline{\omega} - \frac{K}{N}\sum_{j=1}^{N} \sin\left(\phi_i - \phi_j\right) \\
&= \omega_i - \overline{\omega} - \frac{K}{2N\mathrm{i}}\sum_{j=1}^{N}\left[e^{\mathrm{i}(\phi_i-\phi_j)} - e^{-\mathrm{i}(\phi_i-\phi_j)}\right] \\
&= 0
\end{aligned}$$

it follows that:

$$\begin{aligned}
\Delta\omega_i = \omega_i - \overline{\omega} &= \frac{K}{2N\mathrm{i}}\sum_{j=1}^{N}\left[e^{\mathrm{i}(\phi_i-\phi_j)} - e^{-\mathrm{i}(\phi_i-\phi_j)}\right] \\
&\overset{Eq.10}{=} \frac{K}{2\mathrm{i}}\, r\left[e^{\mathrm{i}(\phi_i-\Psi)} - e^{-\mathrm{i}(\phi_i-\Psi)}\right] \\
&= K\, r\, \sin(\phi_i - \Psi)
\end{aligned} \tag{11}$$

where the last two steps can be justified by reminding that

$$r\, e^{\mathrm{i}\Psi} = \frac{1}{N}\sum_{j=1}^{N} e^{\mathrm{i}\phi_j} \implies r(t)\, e^{\mathrm{i}(\Psi-\phi_i)} = \frac{1}{N}\sum_{j=1}^{N} e^{\mathrm{i}(\phi_j-\phi_i)}$$

□

Comment: Having introduced the order parameter in Eq.10 and using the derivation in the above proof pave the way to a different expression for the time evolution of the phase of the oscillator in the Kuramoto system: the interaction term is not expressed any longer as the sum of single oscillator interactions but is now evaluated using the order parameters itself. Given this analytical result and under appropriate conditions which will be introduced later in the report (Sec.3), Eq.11 will be used as starting point for a faster computation of the time evolution of the Kuramoto system.

2.4 Kuramoto model and XY ferromagnetic model

The Hamiltonian introduced in Eq.6 is the same of the one used for the XY *ferromagnetic* model where (with $K > 0$) configurations with spin in magnetic domains (oscillators in the Kuramoto model) pointing in the same direction have a lower global energy and therefore are closer to the equilibrium. Just as in the XY model, a random field can be considered so that frustration can be modelled in a similar way as the one presented for the Kuramoto model.

STATEMENT #5:

Show that the ground state of $\mathcal{H}$ is rotationally invariant also with the presence of the random field.
What result is expected for the Jacobian matrix of the system calculated at the fixed points?
Is $[1, 1, \ldots, 1]$ an eigenvector?

Proof. This analogy suggests another important feature of the extreme points of the Kuramoto model: if in the equations for the time evolution of the phase Eq.3 (or equivalently Eq.5) a uniform translation of the a $\widetilde{\alpha} = mod(\alpha, 2\pi)$ phase is considered for each oscillator, so that $\theta_i \to \theta_i + \widetilde{\alpha}$ $(\phi_i \to \phi_i + \widetilde{\alpha})$, the result obtained in Eq.8 and Eq.9 are still preserved as, given any two ϕ_i, ϕ_j

$$\cos\left(\phi_i - \phi_j\right) \overset{\phi_{i,j} \to \phi_{i,j} + \widetilde{\alpha}}{=} \cos\left(\phi_i + \widetilde{\alpha} - (\phi_j + \widetilde{\alpha})\right)$$

and the random field still remains random if a common phase is added to all the oscillators. On the top of that, as each oscillator keeps the same natural frequency, it results that the time evolution of the system does not change under uniform rotation. This also means that there are in fact an infinite amount of stable state for the Kuramoto systems just like there are infinite ground states in the XY model.

Given this context, it is remarkable and relevant for the later analysis to observe that, as oscillators can be described by unit vectors on the complex plane: this also means that when a given configuration of oscillators is multiplied for a multiplicative factor,

still the resulting configuration must lie on an unit circle and therefore the multiplicative factor may only be a complex phase. This observation can be therefore formulated in the following way:

$$\boldsymbol{\phi}(t) = \begin{pmatrix} e^{i(\phi_1(t))} \\ \dots \\ e^{i(\phi_N(t))} \end{pmatrix} \overset{\phi_i \to \phi_i + \alpha}{\to} R(\alpha) \begin{pmatrix} e^{i(\phi_1(t))} \\ \dots \\ e^{i(\phi_N(t))} \end{pmatrix} = \begin{pmatrix} e^{i(\phi_1(t)+\alpha)} \\ \dots \\ e^{i(\phi_N(t)+\alpha)} \end{pmatrix} = \widetilde{\boldsymbol{\phi}}(t), \ |\alpha| = 1$$

As from the above proof, the systems $\boldsymbol{\phi}$ and $\widetilde{\boldsymbol{\phi}}$ are still characterized by the same time evolution, therefore, given $\boldsymbol{J}$ the jacobian matrix for the system:

$$\boldsymbol{J}(\boldsymbol{\phi}(\boldsymbol{t})) = \boldsymbol{J}(\widetilde{\boldsymbol{\phi}}(\boldsymbol{t})) \iff \boldsymbol{J}\left[\alpha \cdot \begin{pmatrix} 1 \\ \dots \\ 1 \end{pmatrix}\right] = 0 \iff \alpha = 0$$

This last two results in particular show that $\begin{pmatrix} 1 \\ \dots \\ 1 \end{pmatrix}$ is an eigenvector correspondent to uniform rotations of the oscillators in the Kuramoto system. The analysis of its eigenvalue will follow in the next paragraph.

Jacobian matrix analysis When fixed points (Eq.5= 0) are considered

$$\Delta(\omega_i) = \frac{K}{N} \sum_{j=1}^{N} sin(\phi_i - \phi_j)$$

Therefore, the Jacobian **J** (neglecting the K/N factor without loss of generality), the following result is obtained

$$\boldsymbol{J} = \begin{pmatrix} -\sum_{i \neq 1}^{N} cos(\phi_i - \phi_1) & \dots & cos(\phi_1 - \phi_N) \\ \dots & -\sum_{i \neq 2}^{N} cos(\phi_i - \phi_2) & \dots \\ cos(\phi_N - \phi_1) & \dots & -\sum_{i \neq N}^{N} cos(\phi_i - \phi_N) \end{pmatrix} \tag{12}$$

The evaluation and interpretation of eigenvalues and eigenvectors can be computed easily for a low N case: in case N=2 for example, being $x = cos(\phi_1 - \phi_2)$, it yields

$$J = \begin{pmatrix} -x & x \\ x & -x \end{pmatrix}$$

for which there are two possible eigenvectors: $\mathbf{v}_{1,N=2} = \begin{pmatrix} 1 \\ 1 \end{pmatrix}$ with eigenvalue $\lambda_{1,N=2} = 0$

and $\mathbf{v}_{2,N=2} = \begin{pmatrix} -1 \\ 1 \end{pmatrix}$ with eigenvalue $\lambda_{1,N=2} = -2x$. The previous result was then generalized for a N×N matrix and computed: by so doing, it was checked that again the $\mathbf{v}_{1,N\gg1} = [1, 1, \dots, 1]$ was again an eigenvector with correspondent eigenvalue $\lambda_{1,N\gg1} = 0$. From the previous calculations, it also resulted that the $\mathbf{v_{1,N\gg1}}$ eigenvector also was the only one with null correspondent eigenvalue while the remaining eigenvalues from the other eigenvectors are equal to -N.
As a result, the eigenvalues of **J** are negative semidefinite. This last point will have relevant consequences for the analysis of the stability of the system (Sec.2.4). □

Stability analysis and implications In order to characterize the fixed points and relate this analysis to the results from Sec.2.3, second partial derivative test on the $\mathcal{H}$ function must be considered. Note that, from the results in Eq.2.2, it follows that:

$$\boldsymbol{J}(\mathcal{H}) = \mathcal{M}(\boldsymbol{\phi}(t))$$

where $\mathcal{M}$ is the Hessian matrix. This means that eigenvalues of $\boldsymbol{J}(\boldsymbol{H})$ are equal to the eigenvalues of $\mathcal{M}(\boldsymbol{\phi}(t))$ and therefore:

$$det\big[\mathcal{M}(\boldsymbol{\phi}(t))\big] = 0 \tag{13}$$

as one of the eigenvalues of $\boldsymbol{J}(\boldsymbol{\phi})$ has been proved to be equal to zero in the above proof.

This means that, when applying the stability criterion for the characterization of the critical points using $\mathcal{M}$, no useful information is returned from the test. When relating this observation with the question in Sec.2.3, this means that it is not possible to classify the extreme points of the $\mathcal{H}$ function and hence define an asymptotically stable equilibrium. Note this very same result would have been obtained also if the condition in Sec.2.3 ($(\omega_i - \overline{\omega})\forall i = 1, \dots\ N$) was not met.

The following example can be used to acquire an useful insight of the systems dynamics in addition to the Jacobian analysis above.

Starting from Fig.1, it can be easily be understood that if a system is initialized with a degenerate $g(\boldsymbol{\omega})$ *and* in the unstable fixed point $\boldsymbol{\phi}_{unstable} = [0, \frac{2\pi}{N}, 2 \cdot \frac{2\pi}{N}, \dots, 2\pi]$ (namely the N oscillators have phases $2\pi/$N apart), the order parameter will be equal to zero over time and therefore $r_\infty = 0$, regardless of the value of K.
However, when (e.g.) K>K_c, if the oscillators have phases $\boldsymbol{\phi} \neq \boldsymbol{\phi}_{unstable}$, the system will evolve in time towards a more energetically stable configuration and tend to phase locking condition: in this case in fact, as $\mathcal{H}$ is a Lyapunov function, the system will evolve towards a more stable configuration in which $\mathcal{H}$ will be minimized (Fig.1). Note that, without loss

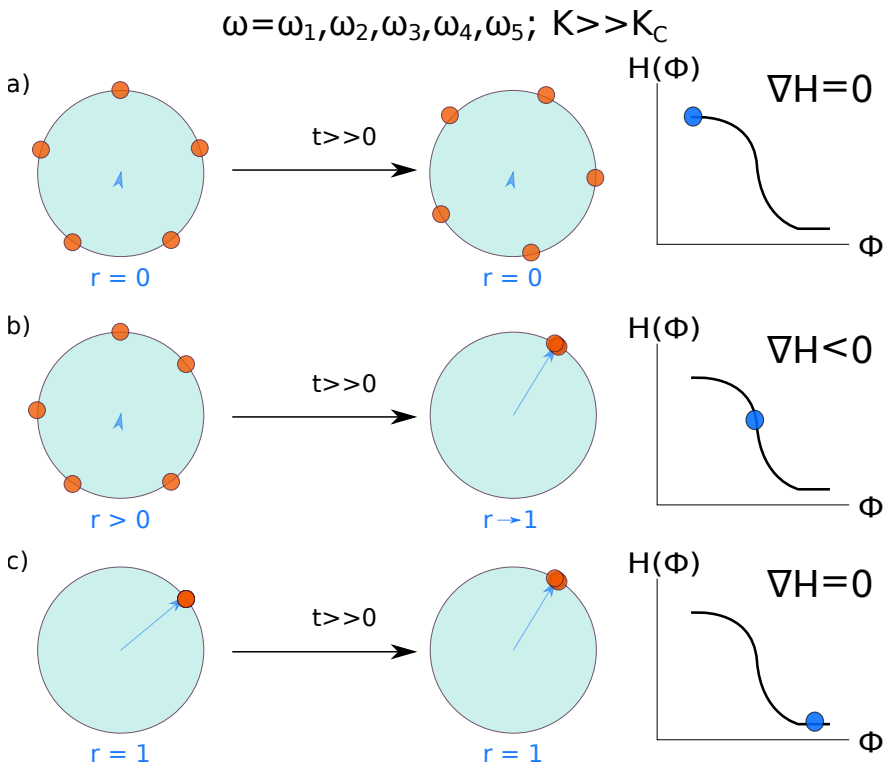

Figure 1: Consider two Kuramoto system with N$=5$ and $\omega_{i=1,\dots,5} = \omega$: a) starting configuration has phases exactly equally spaced: an unstable fixed point is considered and $\nabla\mathcal{H} = 0$; b) initial phases are not equally spaced: the starting configuration is not a fixed point and therefore $\nabla\mathcal{H} < 0$ and the system evolves towards a more stable configuration (minimum for the $\mathcal{H}$ function; c) initial configuration is a fixed point, then $\nabla\mathcal{H} = 0$ and the correspondent fixed point is asymptotically stable.

of generality, these very same results are unchanged if a uniform rotation of the system is considered, as shown in Sec.2.4.

3 Simulation

In addition to the assumption in Eq.2, the following assumptions were made for the simulations:

$$\begin{cases} \boldsymbol{\theta}(0) \in U[0, 2\pi] \\ \boldsymbol{\omega}(0) \in g(\boldsymbol{\omega}), \text{ symmetric about } 0 \end{cases} \tag{14}$$

being $U[0, 2\pi]$ uniform distribution in $[0, 2\pi]$.
The $g(\boldsymbol{\omega})$ distributions used will be a $U[-\gamma, \gamma]$ and $\mathcal{N}[0, 1]$ normal distribution with 0 mean and σ equals to 1 and will be specified for each simulation.
On the top of it, for the $\mathtt{r}_\infty(K)$ plots, a direct comparison with the (r, K) values which

verified the consistency equation

$$1 = K \cdot \int_{\pi/2}^{\pi/2} cos^2(\theta) g\big(K \cdot r \cdot sin(\theta)\big) d\theta \tag{15}$$

was obtained by integrating with a trapezoid method. A bisection algorithm was used for finding the (r, K) combinations which met the conditions in the the following equation. Results will shown a correspondence with simulation results.

Simulation parameters and time evolution algorithm The following notation will be used for the variables of the simulation

- `N`, number of Kuramoto oscillators;
- `T`, ending time for the simulation;
- `dt`, time step;
- `K`, coupling constant of the Kuramoto system simulated;
- r_∞(`K`) order parameter in the last 10% of the simulation for a given `K` value in each run, then averaged between different runs.

Unless differently specified, all results are evaluated starting from the averages over $\mathtt{n}_{runs} = 20$ runs for each given configuration of `N,T,dt,K`: this allowed (already in the preliminary runs) to verify how the noise decreased with increasing `N`.
The algorithm chosen for evaluating the time evolution of the systems was the Euler scheme. Numerical evidence from [4] suggested that, although it is a first-order differences algorithm, the Euler method still returns more than reliable results for the purpose of this investigation. However, differently from [4], a value of `dt`$= .01$ (one order of magnitude smaller than the one used in the paper) was set.
For generating a $\mathcal{N}[0, 1]$ distribution (useful for the setting the initial configuration of ω), the Box-Muller [5] algorithm was used.

***Mean-field* and *non-mean-field* algorithms** [1] Throughout the simulation part, two different equations were implemented in the Euler algorithm for two different purposes and are in List.1:

1. A *non-mean-field* approach: following Eq.3, computational time $\mathcal{O}(\mathtt{N}^2)$].

[1] Note that in fact both approach can be referred as *mean-field* in the sense that all the oscillators feel the same coupling with all the other oscillators in the system. However, for practicality, it will be referred to *non-mean-field approach* when the Eq.3 was considered and *mean-field approach* when $\dot{\theta}(t)_i = \omega_i + K\, r(t)\, sin(\Psi - \theta_i(t))$ was used.

2. A *mean-field* approach: used to investigate the $r_\infty(K)$. Note that computationally speaking, the *mean-field* algorithm does not require the nested `for loop` as the interaction terms evaluation is based directly on the order parameter: as an overall result, the computational times using the *mean-field* approach were $\sim 90\%$ smaller than the one using the *non-mean-field* approach. This resulted in the possibility to explore a `K` resolution up to $0.01 - .005$ while still keeping reasonable enough computational times [computational time $\mathcal{O}(\mathtt{N})$].

```
void EulerStep(float *phases, float *ang_freqs_0, float K, float o_par[]){
  //o_par = Order Parameters, ang_freqs_0 = Natural frequencies
  // o_par[0] == modulus, o_par[1] == Psi
  int i,j;
  double iN = 1./((double)N);
    if(mean_field==false){ //Mutual interaction approach
      for(i = 0;i < N; i++){
        phases[i] = phases[i] + dt * ang_freqs_0[i];
        for(int j = 0; j < N; j++){
            phases[i] += dt * K * iN * sin(phases[j]-phases[i]);
        }
      }
    }
    else{ //Mean field approach
      float interaction_term;
      for(i = 0;i < N; i++){
        //Evaluate interactions
        interaction_term = K*o_par[0]*sin(o_par[1]-phases[i]);
        //Update phases
        phases[i] += (ang_freqs_0[i] + interaction_term)*dt;
      }
    }
}
```

Listing 1: Euler method algorithm for Kuramoto oscillators.

Some preliminary runs were used to get a better insight of the numerical part of this project, in particular:

- To check if the analytical result of Eq.3 (*non-mean-field*) being equal to Eq.1(*mean-field*) was returned also numerically from the code: this was used as a benchmark to validate the robustness of the simulation with the given simulation parameters. It was indeed verified, as expected, that the two equations for the time evolution of the system returned, for fixed parameters and initial conditions, exactly the same numerical values up to the last available `float` digit (order of 10^{-7}).
- Regions of interest were spotted for the measurement of $r_\infty(K)$ and suggested a non uniform sweep over the `K` values. By doing so, it was possible to focus the analysis

for relevant configuration of the Kuramoto system. Note that the *non-mean-field* approach will also be used in Sec.4 for the simulation of the Kuramoto model on Watts-Strogatz graph.

Workflow A complete workflow from the *raw* simulation (`C`) to the automatic output-reading and plotting of the results `Python` was then realized. Moreover, on the very same `C` code, it is easily possible to tune and manipulate the configuration for the run (from the number of oscillators to the specific algorithm for the time evolution and $\boldsymbol{\omega}$ distribution). This resulted in an efficient and flexible simulation part.

Criterion for $\mathtt{K}_c$ For this report, the `K` value that is claimed to be the critical coupling parameter $\mathtt{K}_c$ for the Kuramoto oscillators is the $\mathtt{K}^*$ that returned the $r_\infty(\mathtt{K}^*)$ closeset to $\frac{1}{2}$. An alternative method would have been (e.g.) to claim a `K` value to be $\mathtt{K}_c$ when it returned the largest $\sigma(\mathtt{r}_\infty)$ over the different runs.

Code `C` coding language was preferred over others (`Python` in particular) due to the different characteristic benchmark in computational times[2] (note: `Python3` with `numpy` module was considered, no `Cython` module or other built-in module such as `odeint` was taken into account for this project).

3.1 Results

$r_\infty(K)$ **for** $\boldsymbol{\omega} = \mathcal{N}[0,1]$ This analysis returned a $\mathtt{K}_{c,sim} = 1.600$, only a .2% off the the analytical results from the Kuramoto model $\mathtt{K}_{c,th} \simeq 2\sqrt{(\frac{2}{\pi})} = 1.595$ for the simulated initial conditions, showing good agreement with the theoretical predictions.
Having averaged over 20 different runs for `N`$= 5000$ yielded very little fluctuations when using the mean-field approach. This is the reason why a further analysis on the evolution on $r(t,K)$ was performed on the same output of the runs in Fig.2: in particular, the signal-to-noise ratio ($\frac{S}{N} = \frac{r(t,K)}{\sigma\left(r(t,K)\right)}$ in Fig.3) and $r(t)$ (in Fig.4) were outputted are reported for some selected values of `K`. From Fig.4, it is clearly visible that close to the last part of the simulation, for values of `K` after the equilibration, the $\frac{S}{N}$ varies of several orders of magnitude for the different `K` simulated. It is relevant to remark that the $\frac{S}{N}$ starts at about $5 \cdot 10^2$ for low `K`, then it increases as `K`$\rightarrow 1.5 \sim 1.6$ (closer to $\mathtt{K}_c$ and then increases sharply for increasing `K` over 10^5. This suggests a more disordered behaviour close to the transition

[2] In this case, `benchmarks` are considered: the algorithms in the reference are indicative of the order of magnitude of the different computational times for different coding purpose which can only partially be related to the actual purpose for this code.

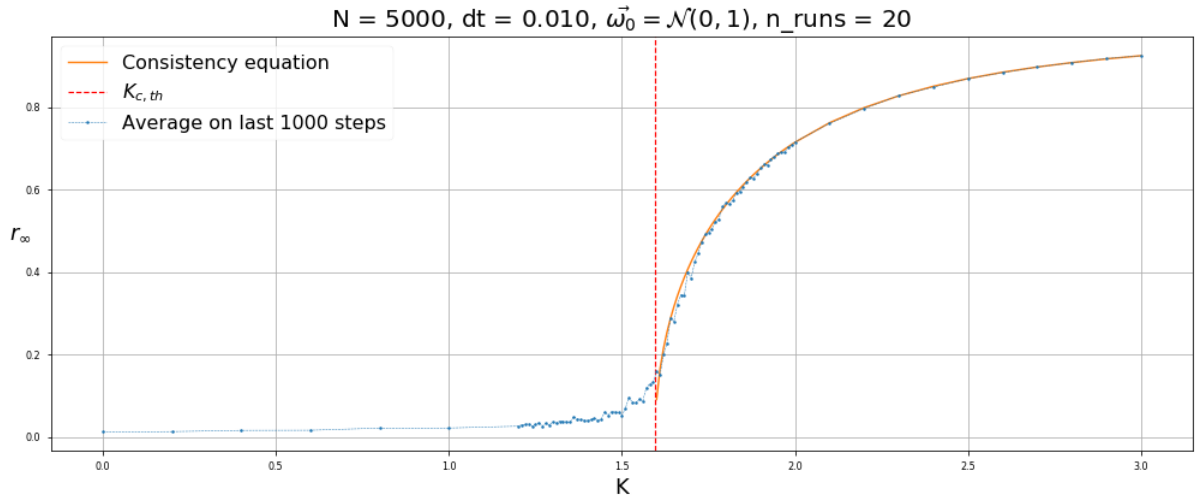

Figure 2: $r_\infty(K)$ for $\boldsymbol{\omega} = \mathcal{N}[0,1]$. As errorbars were not clearly visible, a different quantitative analysis of the variability over different runs is present in Fig.3 and Fig.4. A comparison with the consistency equation Eq.15 is also reported. The same outline will be considered for all others $\mathtt{r}_\infty$ plots.

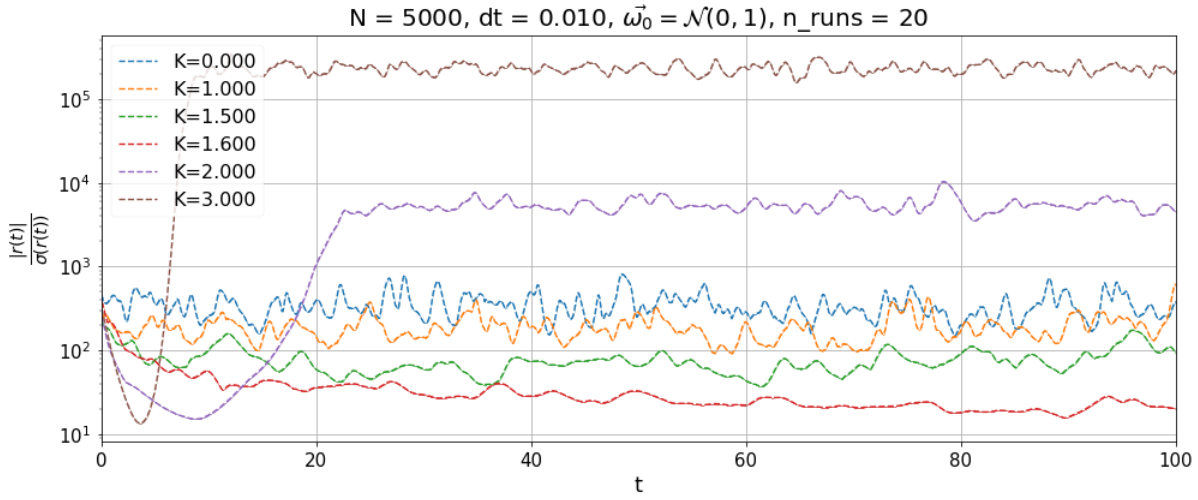

Figure 3: $\frac{r(t,K)}{\sigma\left(r(t,K)\right)}$ for $\boldsymbol{\omega} = \mathcal{N}[0,1]$, mean-field approach

from no phase locking to (partial) phase locking, similar to what is generally seen in the case of a first order phase transition, as suggested from literature[6].

r(t) for `K=1,2` It is interesting to relate Fig.5 with Fig.4 and Fig.2: on the one hand, the values at the end of the simulation in Fig.5 match the ones in Fig.2 (so the "asymptotic" behaviour matches between the two runs, regardless of having a factor 5 different number of oscillators). When comparing Fig.5 and Fig.4, it is apparent that `K`$= 2$ the equilibration

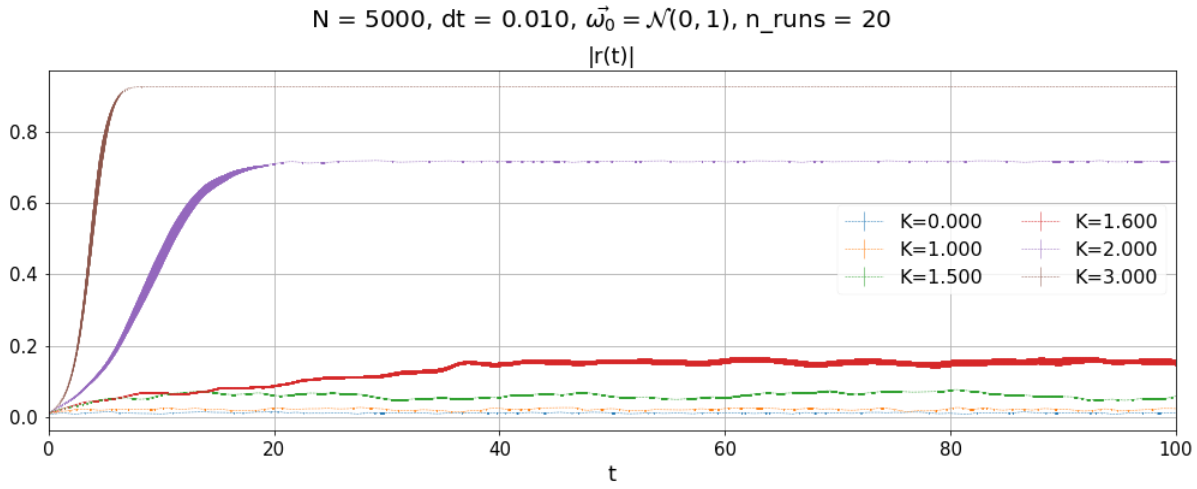

Figure 4: $|r(t,K)|$ for $\omega = \mathcal{N}[0,1]$, mean-field approach. Part of these results can be compared with those in Fig.5 where a non-mean-field approach was used.

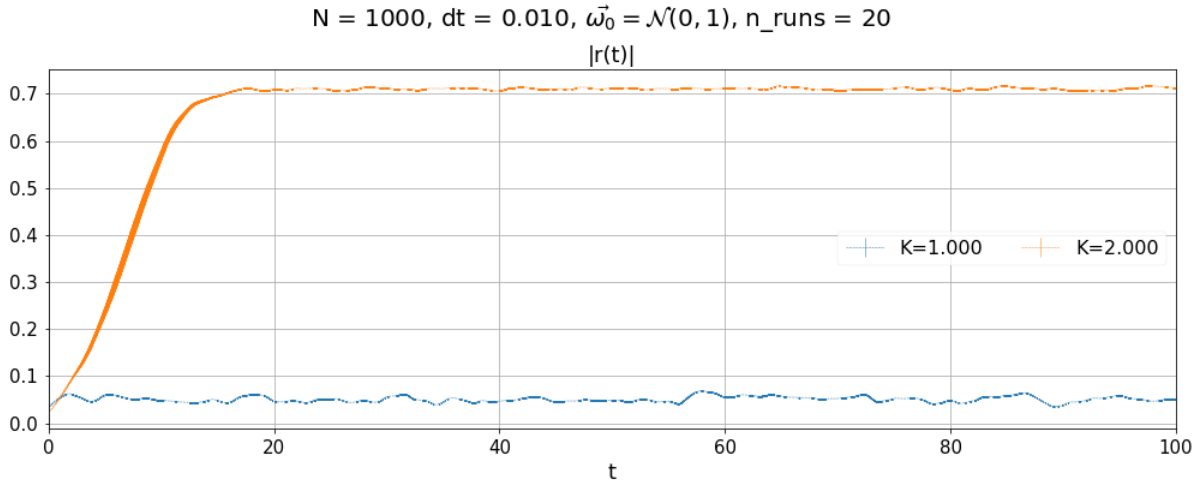

Figure 5: $|r(t;K=1,2)|$ for $\omega = \mathcal{N}[0,1]$, non-mean-field approach. In this case, just like what shown inf Fig.4, it can be seen that the partial synchronization gets more and more pronounced as K exceeds $K_{c,th}$, as summarized in Fig.2.

was reached already at about $t_{N=5000} = 30$ and (mostly, made exception for some ripples which survived also for larger t) $t_{N=1000} = 30$. Also this argument suggests that indeed a simulation of the system for N= 1000 would have yield almost the same results.

Natural frequencies uniformly distributed In this analysis, a $g(\omega = U[-\gamma,\gamma])$ was used and results discussed. In the first part, a $\gamma = .5$ was set, then a comparison for different values of γ was performed and $r_\infty(K)$ for the different γ compared; in the second part a comparative analysis between r(t;K=1) with fixed initial conditions ($g(\omega)$ or θ) was

performed.

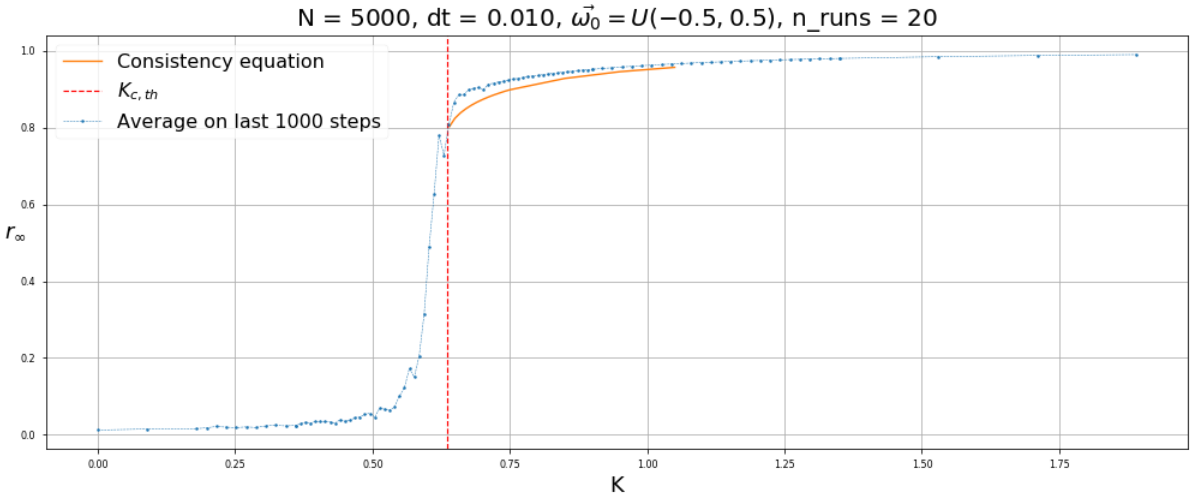

Figure 6: $r_\infty(K)$ for $\omega = U[-.5, .5]$, mean-field-approach. $\mathtt{K}_c = .625$, $\mathtt{K}_{c,th} = .636$

$r_\infty(\mathtt{K})$ The same global behaviour for the $\frac{S}{N}$ in Fig.3 with lower $\frac{S}{N}$ for $\mathtt{K} \to \mathtt{K}_c$ can also be outlined in Fig.7

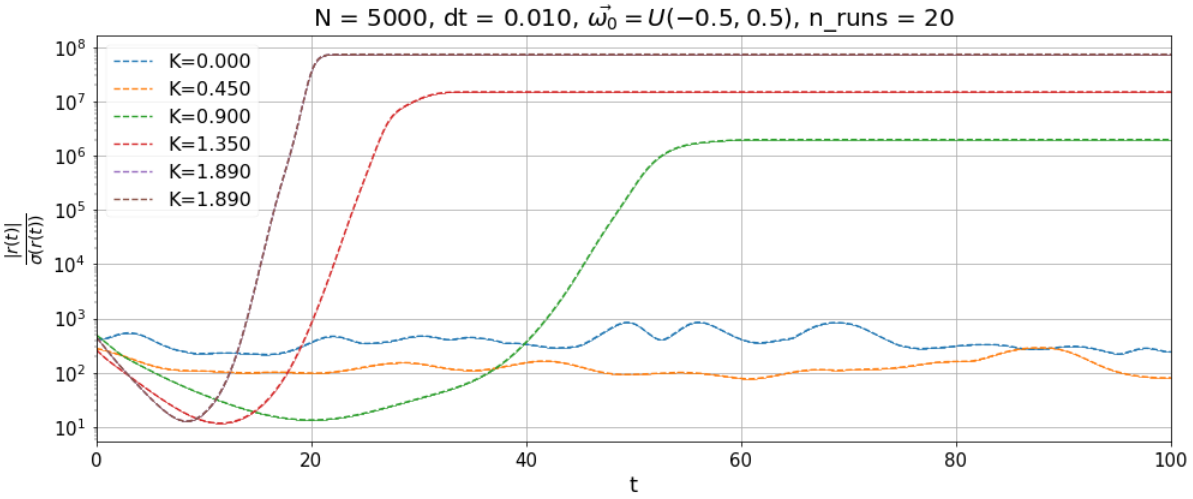

Figure 7: $\frac{r(t,K)}{\sigma\left(r(t,K)\right)}$ for $\omega = U[-.5, .5]$, mean-field approach. Again note that for $\mathtt{K} \to \mathtt{K}_{c,th} = .636$, the $\frac{S}{N}$ remains lower than for other $\mathtt{K}$-s throughout the simulation.

The present analysis showed that $g(\omega) = U[-.5, .5]$ returned a critical value for the coupling parameter is way lower than the one for $g(\omega) = \mathcal{N}[0, 1]$. The very same code was used to explore higher γ values and measure the $\mathtt{K}_c$: results are in Fig.8 and Fig.9 and as $\frac{S}{N}$ in Fig.7 showed the same behaviour as the one in Fig.3. As $\frac{S}{N}$ for $\gamma = 5, 10$ outlined

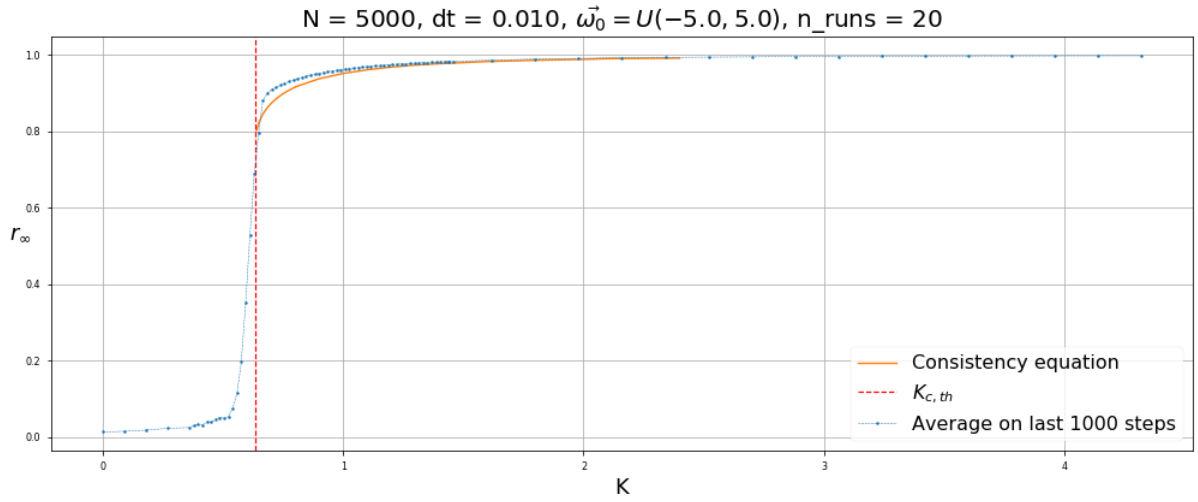

Figure 8: $r_\infty(K)$ for $\omega = U[-5, 5]$, mean-field-approach. $K_c = .625$, $K_{c,th} = .636$

the same behaviour as in Fig.Fig.7, they are not going to be reported. The analysis in Fig.8 and Fig.9 revealed only little differences in the K_c value.
Apart from the K_c value, the great difference with Fig.2 where $g(\omega) = \mathcal{N}[0, 1]$ was used is a kind of *explosive* synchronization of $r_\infty(K)$ close to K_c. Similar analysis in literature suggest that this could be an indicator for a first order phase transition for this particular $g(\omega)$[7].
When comparing the critical values of the coupling parameters, it resulted that

$$1.600 \simeq K_{c,g(\omega)=\mathcal{N}[0,1]} > K_{c,g(\omega)=U[-\gamma,\gamma]} \simeq .636 \tag{16}$$

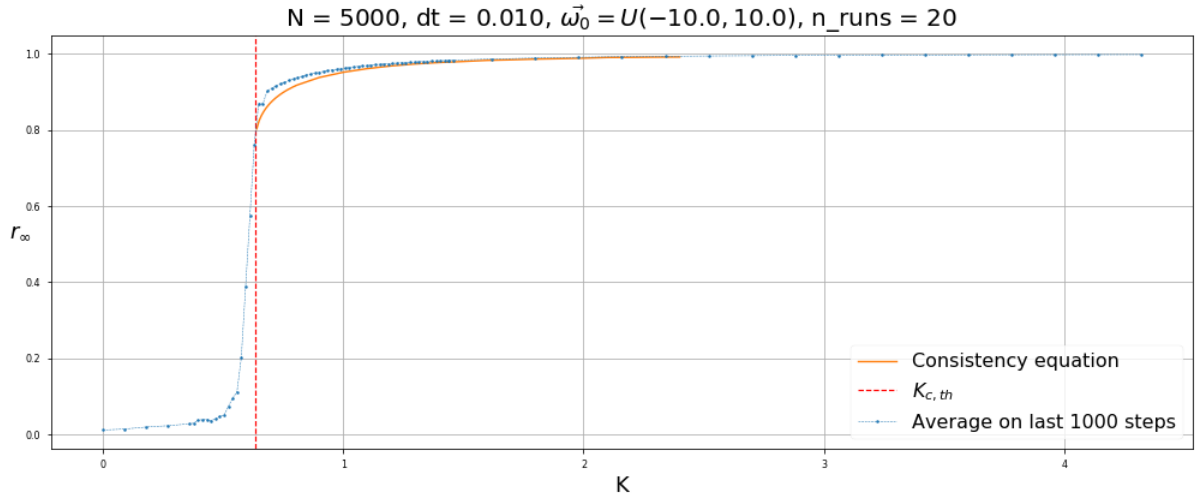

Figure 9: $r_\infty(K)$ for $\omega = U[-10, 10]$, mean-field-approach. $K_c = .625$, $K_{c,th} = .636$

The lower K_c can be explained if the analytical expression for $K_c = \frac{2}{\pi g(0)}$ is considered: as a counter-example, the same simulations for the $g(\omega) = U[-\gamma, \gamma]$ were perfomed for greater values $\gamma = 5, 10$. As expected, the obtained value for the K_c did not change at all as its value is only determined by $g(0)$. Results are in Fig.8 and Fig.9.

Fixed realization of natural frequencies Ten single runs were launched sharing all the same set of natural frequencies for N= 1000, K= 1. Results are in Fig.10. In this case, it

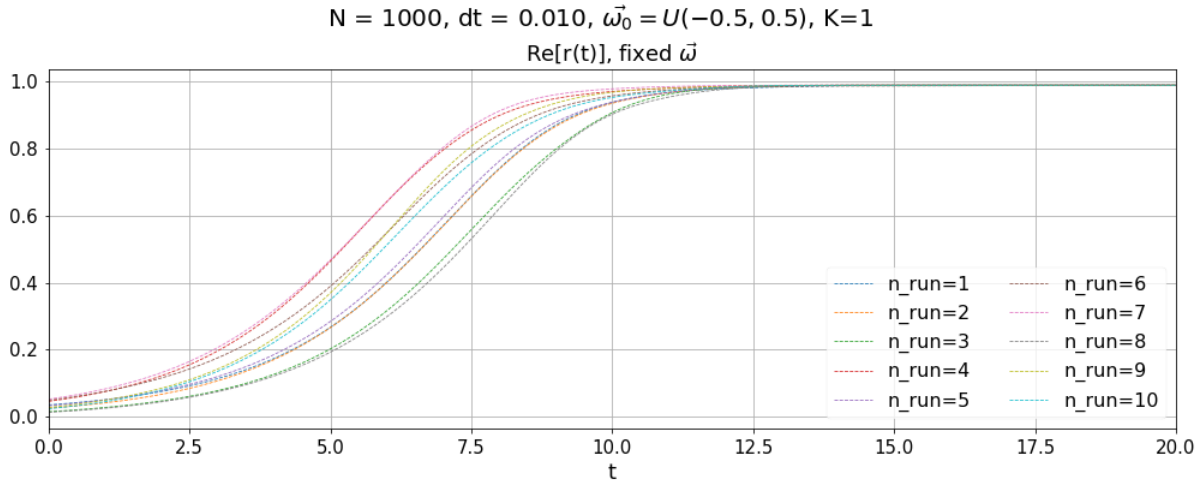

Figure 10: r(t) for 10 different runs, K=1 and fixed natural frequencies. Simulation was performed up to T= 1000 but in this visualization a tmax= 20 is set in order to focus on the important features of this simulation.

can be seen that the order parameter always start at slightly different points between 0 and .1 and that the curves from r(t) show similar behaviour in time (due to the different $\theta = U[0, 2\pi]$ for each run). In addition to that, the fixed $g(\omega)$ results into a similar time evolution where only the different initial configurations of the phases can be accounted for differences in the time evolution of the systems simulated.

Fixed realization of initial phases Differently from the results in the previous case, as all runs now share the same $\theta(0)$, all curves in Fig.11 share the same starting point with $r(t = 0) \simeq .05$. More interestingly, each run has a slightly different $\overline{\omega}$ value due probably to the small numerical fluctuations in the random generation of the $g(\omega) = U[-.5, .5]$ distribution: as a consequence, runs in which the $\overline{\omega}$ was less dispersed converged to the phase locking condition faster than others.
In conclusion, for fixed $\theta(0)$, the different equilibration characteristic times are due only to an initialized ω dispersion: the less dispersed the ω in a given run, the faster the convergence to the equilibrium. As a thought counter-example, consider the case of a

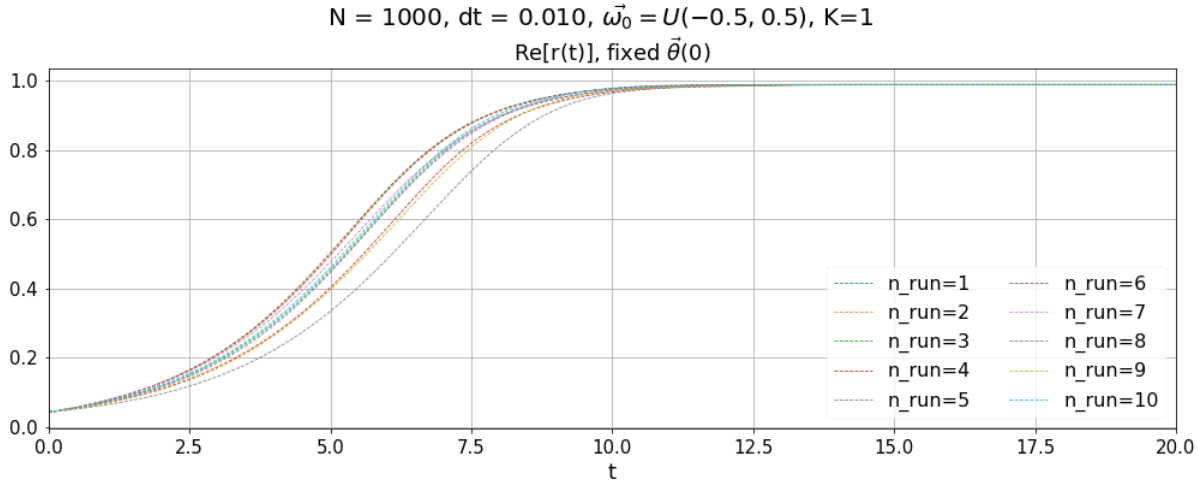

Figure 11: r(t) for 10 different runs, `K=1` and fixed initial phases, non-mean-field approach. Simulation was performed up to `T`= 1000 but in this visualization a `tmax`= 20 is set in order to focus on important on the features of this simulation.

degenerate $\boldsymbol{\omega}$ and fixed $\boldsymbol{\theta}(0)$: in this case all rising times would have been the same and the resulting `r`(t) plot would have been above any other possible `r`(t) curve.

Comment: Fig.10 and Fig.11 show that before the equilibration of the system, for the simulated conditions:

- The average value of the order parameter is higher for fixed $\boldsymbol{\theta}(0)$ when compared with the simulations with fixed $\boldsymbol{\omega}(0)$ at the same simulation time (e.g. $t = 5$).
- Results from the simulation with fixed $\boldsymbol{\theta}(0)$ seem less dispersed when compared with results with $\boldsymbol{\omega}(0)$ in Fig.10.

A potential explanation for this two features can be found if the Eq.3 is taken into account. On the one hand, the different initial phases have a large contribution to the interaction term: the interaction is not in fact just driven by an individual phase of an oscillator, but by all pairs of relative phases differences of each oscillator with every other in the system. As a consequence, the interaction term can largely differ between two different simulation initialized with different $\boldsymbol{\theta}(0)$. On the other hand, the contribution of different ω distributions only dictate a constant term which regards the same individual oscillator in Eq.3: this is maybe the reason why it results a less dispersed time evolution of $\mathtt{r}(t)$ for fixed $\boldsymbol{\theta}(0)$ and variable $\boldsymbol{\omega}$ than what found for fixed $\boldsymbol{\omega}$ and variable $\boldsymbol{\theta}(0)$.

However, a more exhaustive simulation would have been needed in order to outline the overall importance of fixed initial phases or natural frequencies in a Kuramoto system simulation: as an example, it would have been possible to run blocks of several runs with

a fixed initial conditions (e.g. 10 different blocks of simulations with 10 different initialized ω, having a random phase distribution initialized for each of the 10 runs within each block). Then, by averaging results from different blocks, it would have been probably possible to outline the behaviour of this scenario in a more quantitative and robust way.

4 Kuramoto model on Watts-Strogatz graph

4.1 Outline of the model

In the above theoretical analysis and simulations, it was supposed that each of the `N` Kuramoto oscillators was interacting with every other oscillator in the system. Nonetheless, it is possible to regard the system of interacting Kuramoto oscillators as vertices on a graph and let two oscillators interact only if there is an edge between the correspondent vertices. In Sec.2 and Sec.3 therefore, a Kuramoto systems of oscillators on a fully connected graph has been so far investigated.
For this last part of the project instead, the Kuramoto model on a Watts-Strogatz (WS) graphs is going to be analyzed.
It is meaningful for the later interpretation of the results to recall some crucial features of the WS model:

- $p \to 0$**:** only *local* connections are enhanced. For a Kuramoto system simulated with rewiring probability p, this will result in only adjacent oscillators to be interacting with one another. Note that for values of $\mathtt{N} ggr_{WS}$, this can result in different regions of the graph being in two completely different phases, due to the large shortest path length between non adjacent vertices in the WS graph. In this case ($p \neq 0$ and $p \to 0$), only an infinite (high) value of `K` will allow a *global* synchronization of the system leading to the phase locking condition.

- $p \simeq .5$**:** local and non-local connections are both present in the graph. This results in an high clustering coefficient *and*, at the same time, small shortest path length: it is therefore expected that the critical value for the coupling parameter needed for a phase locking condition will rapidly decrease from the case of $p = 0 \to p \sim .5$ and beyond.

- $p \to 1$**:** The graph tend to a random graph, therefore the network is characterized by small clustering coefficient and small shortest path length: this means that for each vertex in the graph, the number local edges (edges with closest oscillators) is, ideally, zero and it is much easier for the system to enter a phase locking condition for lower $\mathtt{K}_c$.

4.2 Simulation

The workflow for this scenario was organized in a slightly different way:

- The main `Python` code for the generation of WS graphs from the last assignment was modified in order to return a list of edges in the same format as the one provided on `SNAP`[3].
  WS graphs were generated for:
  - `N=2000` vertices;
  - Number of symmetric edges with closest neighbours before the rewiring $\mathtt{r}_{WS} = 3$;
  - Rewiring probability $\vec{p} = [0, 0.05, 0.1, 0.2, 0.3, 0.4, 0.5, 0.6, 0.7, 0.8, 0.9, 0.95, 1]$

  Note that, for a given p value, all the simulations for the Kuramoto system on WS graphs were performed starting from the same WS network.
- The edge list generated for each p was then imported into the main `C` code and used as a reference map for connected edges in the `EulerStep` function as shown in List.2. For these simulation, $\mathtt{n}_{runs} = 10$, `T`$= 200$, `dt`$= 0.01$ parameters were used. Just like in the previous case, the `C` code returned the values of the order parameter over time, averaged over the different runs throughout the time evolution of the system.
- Results from the simulation of the Kuramoto system on the WS graph for $\vec{p}$ imported in `Python`: the heatmap of $\mathtt{r}_\infty(\vec{p}, K)$ in Fig.12 and $K_c(p)$ in Fig.13 were then studied.

```
void EulerStep(float *phases, float *omega0,
      float K, float o_par[], struct adj_edges edges_f)
{
  //o_par = Order Parameters, ang_freqs_0 = Natural frequencies
  // o_par[0] == modulus, o_par[1] == Psi
  int i,j;
  for(i = 0;i < N; i++){  //Update phase with natural frequencies
    phases[i] = phases[i] + dt * ang_freqs_0[i];
  }

  for(i = 0; i< N *(int)(r_WS);i++)
    { // Update with interactions
        phases[edges_f.from[i]] += dt * K * 1./(2.*r_WS)
            * sin(phases[edges_f.to[i]]-phases[edges_f.from[i]]);
    }
}
```

Listing 2: Euler method algorithm for Kuramoto oscillators on WS graph.

[3]This paved the way for simulations of Kuramoto oscillators also on real networks with the very same code.

4.3 Results

For this analysis, results have been obtained using a different $\boldsymbol{\omega} = \mathcal{N}[0,1]$ and $\boldsymbol{\theta}(0) = U[0,2\pi]$ on each run.

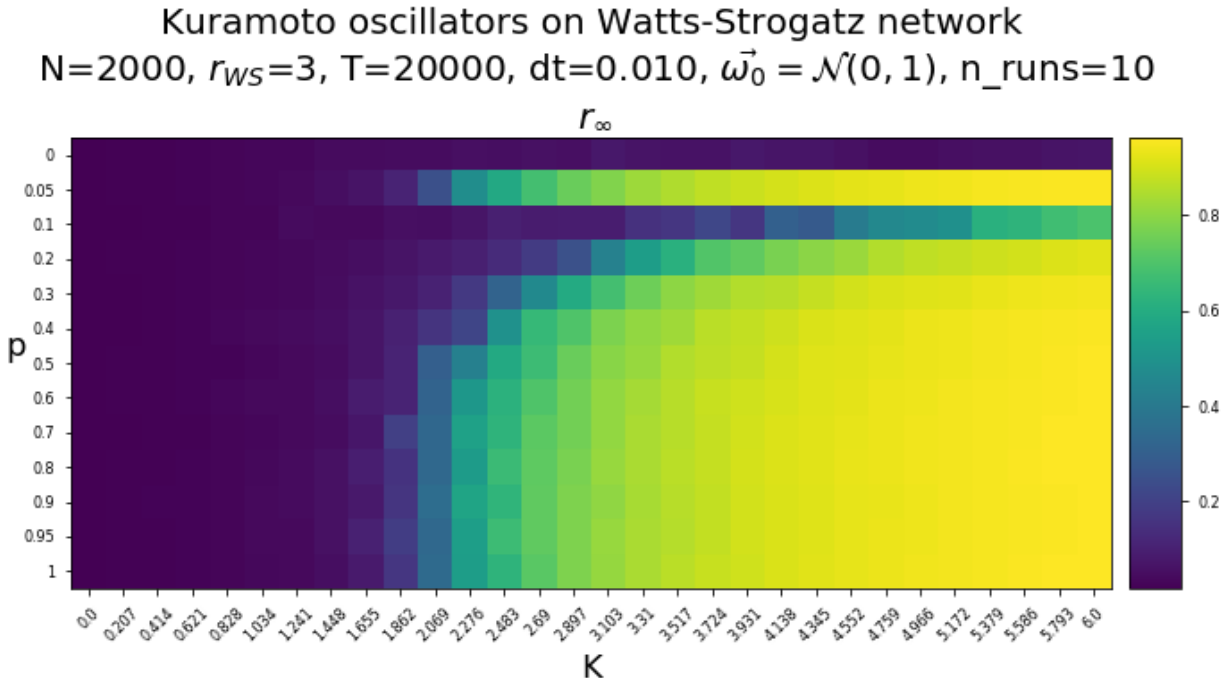

Figure 12: Heatmap representative of the values of $\mathtt{r}_\infty$ for a WS graph with $\mathtt{r}_{WS}$=3.

Fig.12 suggests that, for $p = 0$, only *local* interactions between oscillators in the Kuramoto system on WS graph can take place and thus, a fully synchronized state is never reached (a $\mathtt{K}_c = \infty$ would be needed): this results in a zero order parameter even with the highest simulated K value.

Notice that, apparently, an exception must be made for the values correspondent to $p = .05$ as higher values of $\mathtt{K}_c$ were expected for this specific p value.
However, a possible explanation for the the uncorrect (according to the literature cases) behaviour of the $\mathtt{K}_c(p = .05)$ can be provided if the individual $\mathtt{r}(t, p, K)$ (Fig.16) plots are studied: by doing so, it is clear that for lower values in p, a much greater time scale was needed in order to observe an equilibration of the system into a stable configuration and therefore evaluating a proper $\mathtt{r}_\infty$ value. In addition to that, it was also observed that the equilibration time decreased with increasing values of K. As a consequence, runs for low values of p should have been simulated with much greater values of K and T in order to derive reliable results for the $\mathtt{r}_\infty$ value. This is the main reason why the simulations for $p = .05$ reported here yields results for the $\mathtt{r}_\infty(p = .05, K)$ which are, in fact, not comparable with the ones from other $\mathtt{r}_\infty(p \neq .05, \mathtt{K})$. Nevertheless, for increasing values in p and fixed K values, it can be seen that the higher the p, the lower the $\mathtt{K}_c$ value. This can

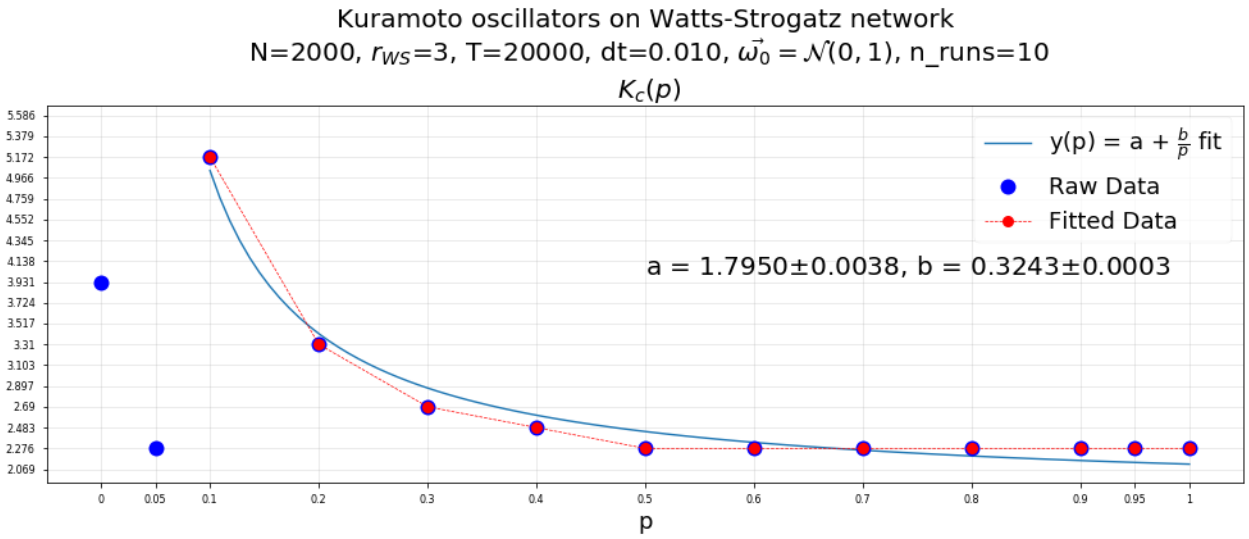

Figure 13: $\mathtt{K}_c(p)$ for a WS graph with $\mathtt{r}_{WS}$=3. Note that the fit has been performed only on the highlighted part of the data. Results differ from literature [8] [$a = 1.64(4), b = 0.28(1)$], even when errors on the fit coefficients are considered, although in the paper a larger dt= .05 and (more importantly) values are measured by simulating over different N size of the network and using the finite-scale method.

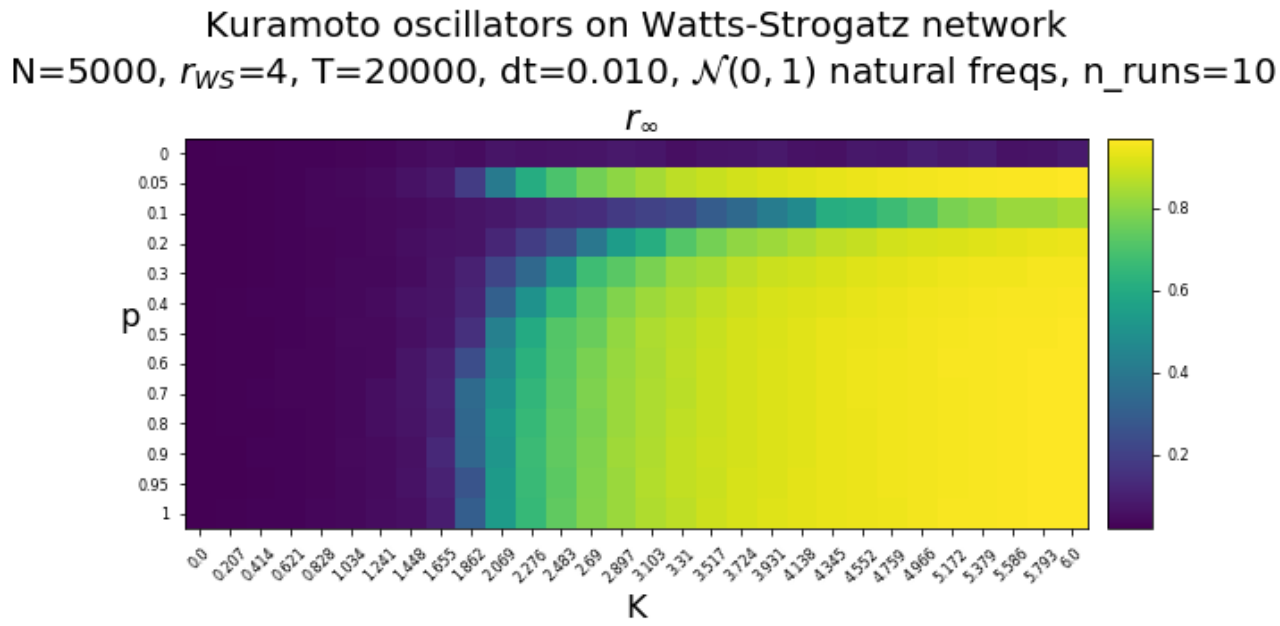

Figure 14: Heatmap representative of the values of $\mathtt{r}_\infty$ for a WS graph with $\mathtt{r}_{WS}$=4.

be seen if the "*iso-*r_∞" curve at $\mathtt{r}_\infty = .5$ is considered.
The values of $\mathtt{K}_c$ with respect to the rewiring probability p have been summed up in Fig.13. A $\frac{1}{p}$ behaviour seems to be fitting the data (as suggested in [8]) for values in $p > .1$.

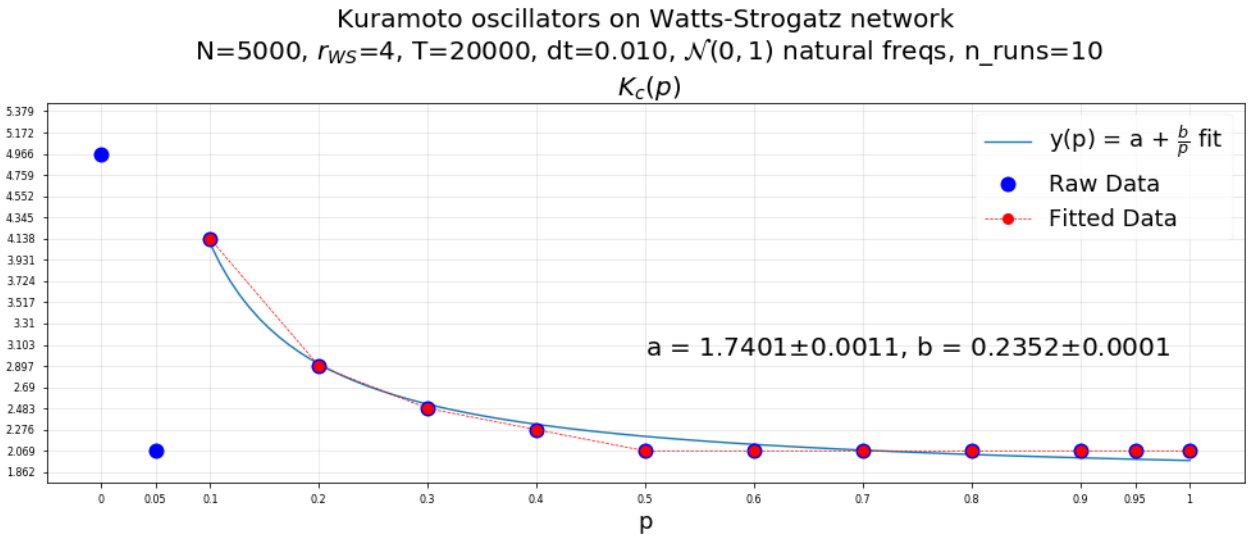

Figure 15: $\mathtt{K}_c(p)$ for a WS graph with $\mathtt{r}_{WS}$=4. Note that the values for b in the fit is lower than the one in Fig.13 has been performed only on the highlighted part of the data.

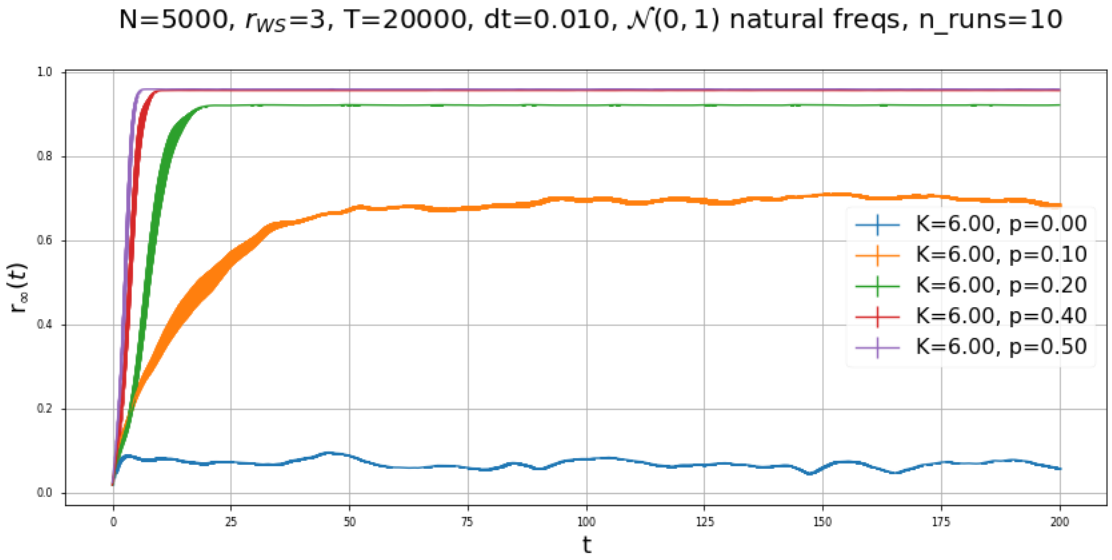

Figure 16: $\mathtt{r}_\infty(t)$ for different values of p and fixed $\mathtt{K}$= 6 (maximum value simulated). This figure was meant just to be a qualitative representation of how the different characteristic time scales for the equilibration depended on the rewiring probability p. Therefore, only results with values of $p > .05$ will in general will a reliable approximation of the $\mathtt{r}_\infty$ value and used in later analysis. This is mostly the reason why the values in Fig.13 and Fig.15 are also not to be considered reliable for low values of p ($p < .05$).

It is expected that the $\mathtt{K}_c$ value for any given $p \neq 0$ will be lower for increasing values of r_{WS}: this can justified by considering that the number of rewired edges grows linearly with $\mathtt{N}$. Therefore, for fixed $\mathtt{N}$ and p, the local behaviour of small and close together clusters of

Kuramoto oscillators will be more and more affected by the number of rewired edges: as a consequence, for fixed N and p, K, there will be increasing $\mathtt{r}_\infty$ for increasing r_{WS}. Results of this analysis are in Fig.14 and Fig.15.

Further Analysis

After a more robust optimization, the present work could be exploited as a foundation for further research on some of the traits of the model which were not investigated in the present work, such as:

- A systematic study not only the modulus of the order parameter, also its Fourier spectrum: during the individual runs it was in fact possible to spot ripples of the $\mathtt{r}(t \to T, K)$ which decreased in amplitude and increased in frequency with growing values of K. It can be speculated that a different spectrum for different K should be observed and maybe some interesting consideration may be inferred by studying at the different spectra for the different coupling regimes.
- An investigation variations of K *within* the same simulation, both in increasing and decreasing the coupling parameter: by so doing, it would be probably possible to study the characteristic equilibration times and hysteresis in the $\mathtt{r}_\infty(\mathtt{K})$ in order to reproduce and then explore results in [7].

5 Conclusions

The most crucial features of the Kuramoto model have been presented and analyzed in the Sec.2: particular effort has been spent on the analysis of the $\mathcal{H}$ function of the system and similarities with the XY model have been suggested. A comment on the stability of the investigated stable states has been conducted, based on the analysis of the critical point for $\mathcal{H}$.

In Sec.3, different scenarios for different parameters of the Kuramoto model have been simulated and results discussed, trying always to relate the observed results with the theoretical analysis of the previous section.

In the last part of the report, a variation of the classical Kuramoto model was explored: a WS graph was created and used to map the interactions between the oscillators in the Kuramoto system. The dynamic of the system for different simulation parameters was simulated and results discussed and compared with a bibliographic reference were the same system was simulated.

References

[1] Kuramoto, Yoshiki and Araki, 1975,
Lecture Notes in Physics, International Symposium on Mathematical Problems in Theoretical Physics, 39. Springer-Verlag, New York. p. 420.

[2] Breakspear, Heitmann and Daffertshofer, 2010,
Generative models of cortical oscillations: neurobiological implications of the Kuramoto model, Front. Hum. Neurosci.
https://doi.org/10.3389/fnhum.2010.00190

[3] Wiesenfeld, Colet and Strogatz, 1998,
Frequency locking in Josephson arrays: Connection with the Kuramoto model, Phys. Rev. E 57, 1563
https://doi.org/10.1103/PhysRevE.57.1563

[4] Sakaguchi, Shinomoto and Kuramoto, (1987),
Local and Global Self-Entrainments in Oscillator Lattices, Prog. Theor. Phys. Vol. 77, No.5, May 1987, Progress Letters
https://doi.org/10.1143/PTP.77.1005

[5] Thomas, Luk, Leong and Villasenor, (2007),
Gaussian random number generators, ACM Comput. Surv. 39, 4, Article 11
https://doi.org/10.1145/1287620.1287622

[6] Pazó, (2005),
Thermodynamic limit of the first-order phase transition in the Kuramoto model, Physical Review E 72(4 Pt 2):046211
https://doi.org/10.1103/PhysRevE.72.046211

[7] Ghosh and Gupta, (2013)
Relaxation dynamics of the Kuramoto model with uniformly distributed natural frequencies, Physica A 392, 3812
https://doi.org/10.1016/j.physa.2013.03.037

[8] Hong and Choi, (2001)
Synchronization on small-world networks, (2001), Physical Review E, Volume 65, 026139
https://doi.org/10.1103/PhysRevE.65.026139